High Efficiency Deep Ultraviolet Light-Emitting Diodes With Polarity Inversion of Hole Injection Layer

Xu Liu, Shengrui Xu, Hongchang Tao, Yanrong Cao, Xinhao Wang, Hengsheng Shan, Jincheng Zhang, and Yue Hao, *Senior Member, IEEE*

***Abstract*—In this work, we investigate the performance improvement of N-polar AlGaN-based deep ultraviolet light-emitting diodes (DUV LEDs) by the inversion of the hole injection layer from N-polar to Ga-polar. The influence of different inversion points on the performance and the energy band of DUV LED is systematically studied, and the principle of performance improvement of DUV LED is explained in detail through the analysis of the energy band. Furthermore, according to the simulation results and practical application, an appropriate inversion point is selected. Under the current of 120 mA, with polarity inversion of the hole injection layer, the light output power of the DUV LEDs increases from 21.34 mW to 29.71 mW, and the applied voltage reduces from 16.06 V to 9.63 V. The DUV LED with polarity inversion has a 132% increase in wall-plug efficiency (WPE) compared with the DUV LED which is totally along [000-1] direction. Therefore, polarity inversion is an effective way to achieve high-performance UV-LEDs.**

***Index Terms*—Deep-ultraviolet (DUV), light-emitting diodes (LEDs), polarity inversion.**

I. Introduction

ALGAN-BASED deep ultraviolet light-emitting diodes (DUV LEDs) have attracted extensive attention in recent years due to their widespread application in many fields, including air sterilization, surface disinfection, ultraviolet (UV) curing and printing, phototherapy and medical applications [1], [2], [3], [4]. Compared with traditional UV light sources, AlGaN-based LEDs feature advantages of low pollution, low energy consumption, long life, and small size [5]. However, UV-LEDs suffer a poor luminous efficiency, and its external quantum efficiency (EQE) and wall-plug efficiency (WPE) are generally lower than 10% and 5%, respectively. Although many efforts have been made to improve the performance of UV LEDs [6], [7], [8], [9], [10], [11], [12], the high-power, high-efficiency, and long-life DUV LEDs are still difficult to achieve.

N-polar LEDs have the reversed polarization field over Ga-polar counterpart, and its unique properties are beneficial to increase the injection efficiency of electrons and holes [13], [14], [15], [16], [17]. Therefore, N-polar LEDs have attracted much attention in recent years. High-quality N-polar III-nitrides films can be obtained in some ways such as substrate orientation, surfactants, and optimized growth conditions [18], [19], [20]. But the high oxygen incorporation rate in N-polar material which is at least 10 times higher than that in Ga-polar material leads to a high oxygen impurity concentration [21], [22]. As shallow donors, the oxygen impurity will lead to high background carrier concentration in III-nitrides, where hole concentration will be adversely affected. Early researchers found that N-polar GaN could be inversed to Ga-polar GaN by heavily doping with Mg or exposing to Mg flux, and the formation of an Mg_xN_y compound was considered to be the cause of the polarity inversion [23], [24], [25], [26], [27]. Thus, the problem of low hole concentration in N-polar LEDs can be solved by polarity inversion. However, there is no studies related to the application of polarity inversion in N-polar UV-LEDs, and the mechanism of polarity inversion in energy band engineering is still unclear. In this study, the enhanced performance of N-polar UV-LED with polarity inversion is numerically investigated. And according to the energy band diagrams and carrier distributions obtained by simulation, the mechanism of the enhanced performance of UV-LEDs with polarity inversion is theoretically analyzed.

II. Simulation Settings

The simulated device structure of UV-LEDs along [000-1] direction is designed and shown in Fig. 1(a). The layer structure includes: a 2-μm-thick n-$Al_{0.6}Ga_{0.4}N$ (Si: 8×10^{18} cm^{-3}) layer is on the sapphire substrate as the electron injection layer. Subsequently, five periods of $Al_{0.57}Ga_{0.43}N/Al_{0.47}Ga_{0.53}N$ are deposited on n-$Al_{0.6}Ga_{0.4}N$ as the multiple quantum wells (MQWs) active region, where the thickness of $Al_{0.47}Ga_{0.53}N$ quantum well is 3 nm, and the thickness of $Al_{0.57}Ga_{0.43}N$

Manuscript received 10 January 2023; revised 14 February 2023; accepted 17 February 2023. Date of publication 22 February 2023; date of current version 6 March 2023. This work was supported in part by the National Natural Science Foundation of China under Grant 62074120, in part by State Key Laboratory on Integrated Optoelectronics under Grant IOSKL2018KF10, in part by the Natural Science Basic Research Program of Shaanxi under Program 2023-JC-JQ-56, and in part by the Fundamental Research Funds for the Central Universities under Grant JB211108. *(Corresponding authors: Shengrui Xu; Yanrong Cao.)*

Xu Liu, Shengrui Xu, Hongchang Tao, Xinhao Wang, Jincheng Zhang, and Yue Hao are with the State Key Discipline Laboratory of Wide Band Gap Semiconductor Technology, School of Microelectronics, Xidian University, Xi'an 710071, China (e-mail: xliu23@stu.xidian.edu.cn; srxu@xidian.edu.cn; hchtao@stu.xidian.edu.cn; wangxinhao@stu.xidian.edu.cn; jchzhang@xidian.edu.cn; yhao@xidian.edu.cn).

Yanrong Cao is with the School of Mechanical and Electrical Engineering, Xidian University, Xi'an 710071, China (e-mail: yrcao@mail.xidian.edu.cn).

Hengsheng Shan is with the Materials Institute of Atomic and Molecular Science, Shaanxi University of Science and Technology, Weiyang University Park, Xi'an 710021, China (e-mail: hsshan@sust.edu.cn).

Digital Object Identifier 10.1109/JPHOT.2023.3247451

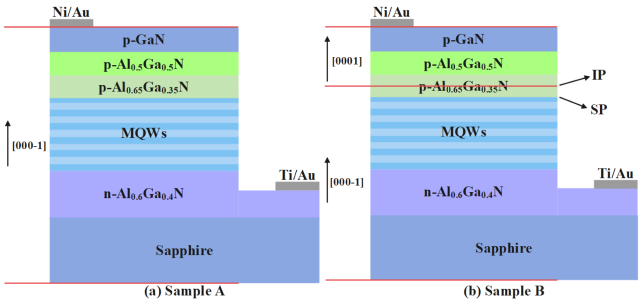

Fig. 1. Structures of (a) Sample A and (b) Sample B.

quantum barrier is 12 nm. The electron blocking layer (EBL) used to suppress electron leakage is a p-type $Al_{0.65}Ga_{0.35}N$ (Mg: 4×10^{18} cm^{-3}) layer whose thickness is 20 nm. Lastly, the thickness of the p-$Al_{0.5}Ga_{0.5}N$ (Mg: 4×10^{18} cm^{-3}) layer is 50nm, and the thickness of the p-GaN (Mg: 2×10^{19} cm^{-3}) layer is 120 nm. The device size is 400 μm $\times$ 400 μm.

In this study, the numerical calculation is performed by Advanced Physical Models of Semiconductor Devices (APSYS), which is an advanced simulation software for semiconductor device physical models. The energy bandgap of the $Al_xGa_{1-x}N$ alloy is obtained by using the following formula [28],

$$E_g(Al_xGa_{1-x}N) = x \cdot E_g(AlN) + (1-x) \cdot E_g(GaN) - b \cdot x \cdot (1-x) \quad (1)$$

where the bandgaps of AlN and GaN are 3.420 eV and 6.026 eV at 300 K, respectively. The bending coefficient b is set to be 1. The energy band offset ratio of the AlGaN based heterojunction is set to be 65:35 [29]. Moreover, the Auger recombination coefficient and the Shockley-Read-Hall (SRH) recombination lifetimes are set to be 1.5×10^{-30} cm^6/s and 10 ns, respectively. According to Fiorentini's theory [30], the shielding coefficient of the theoretical polarization charges is set to be 50% in this study due to the fact that defects and dislocations will compensate part of the polarization charges. Furthermore, we set the temperature and light extraction efficiency (LEE) to be 300 K and 10%, respectively. The other material parameters of the nitrides can be found in other studies [28]. The peak emission wavelength of the calculated electroluminescence (EL) spectra of this UV-LED is around 274 nm at 120 mA.

In the actual growth of the device, although heavily doping with Mg can achieve the inversion from N-polar to Ga-polar, the polarity inversion can't occur instantaneously. Complete inversion can only be achieved after growing a certain thickness of layer [25]. Therefore, complete inversion occurs in the hole injection layer, not at the interface between the active region and the hole injection layer. We define the position where complete polarity inversion occurs as Inversion Point (IP). It is assumed that the layers below IP are N-polar ([000-1]), while the layers above IP are Ga-polar ([0001]). As shown in Fig. 1, we define the interface position between the active region and the hole injection layer as Starting Point (SP). The whole structure grown along [000-1] direction is set as the original LED structure, and different samples can be obtained according to the distance between IP and SP.

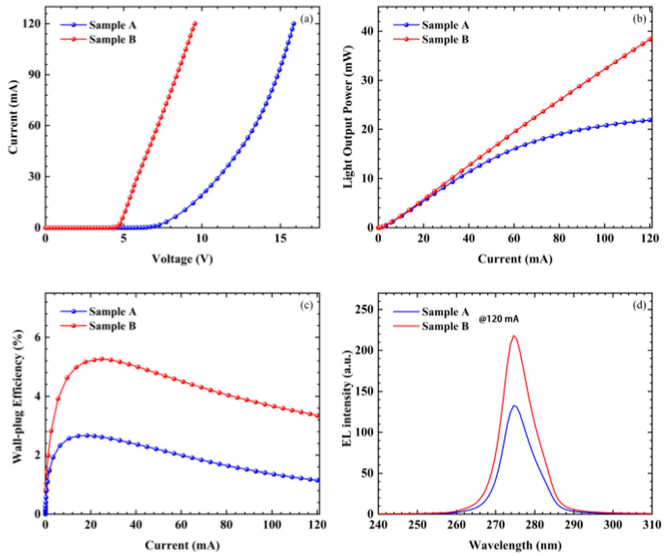

Fig. 2. (a) I-V, (b) L-I curves, (c) WPE and (d) electroluminescence spectra of Sample A and B at 120 mA.

III. Results and Discussion

The original LED structure is denoted as Sample A. The structure in which the distance between IP and SP is 10 nm, that is, the polarity inversion is assumed to occur in the EBL, is denoted as Sample B. As shown in Fig. 1, Sample A and B are identical except for the different polarity in the hole injection layer. And the simulation results of Sample A and Sample B including current and voltage (I-V) curve, light output power-current (L-I) curve, WPE and EL spectra are present in Fig. 2. The turn-on voltages of Sample A and B are about 4.6 V and 4 V, respectively. This means that Sample A needs a larger applied voltage than Sample B to reach the same current value. The voltages of Sample A and B is 15.9 V and 9.55 V at 120 mA, respectively. As the L-I characteristic shown in Fig. 2(b), Sample B has a larger curve slope than Sample A. At the injection current of 120 mA, the light output power (LOP) of Sample B is increased by 75.1% compared with that of Sample A. Furthermore, in order to identify the comprehensive effects of applied voltage and light output power on device performance, the WPE of the two samples are calculated and shown in Fig. 2(c) Over the entire current range, the WPE of Sample B is much higher than that of Sample A due to the decreased applied voltage and the increased LOP. The WPE of Sample B is more than twice that of Sample A at 120 mA. It can be seen from Fig. 2(d) that the EL peak emission wavelength for both samples is around 274 nm, and Sample B has a higher intensity. These results indicate that the polarity inversion of the hole injection layer is helpful to improve the efficiency of devices.

To investigate the performance improvement with the polarity inversion, the carrier distribution profiles of the active region of Sample A and B are characterized. As shown in Fig. 3(a) and

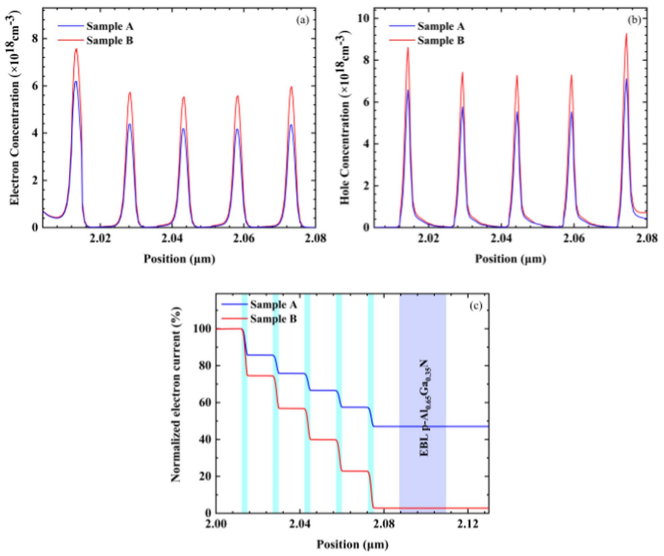

Fig. 3. (a) Electrons and (b) holes concentration distributions among MQWs for Sample A and B at 120 mA. (c) Normalized electron current profiles at 120 mA for Sample A and B.

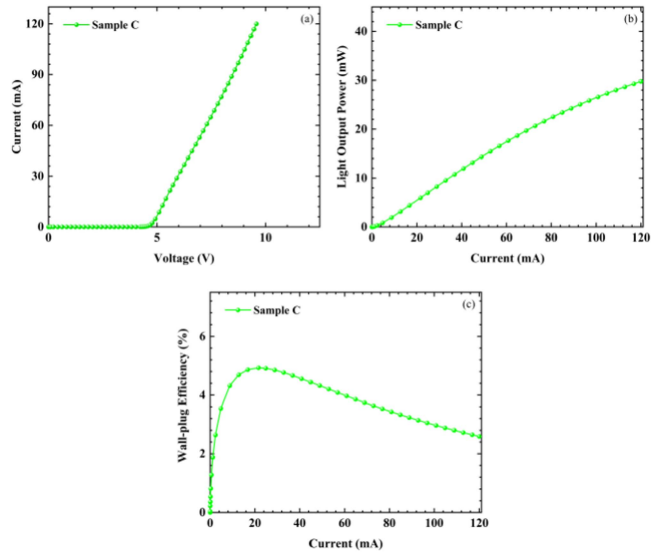

Fig. 5. (a) I-V, (b) L-I curves, and (c) WPE of Sample C.

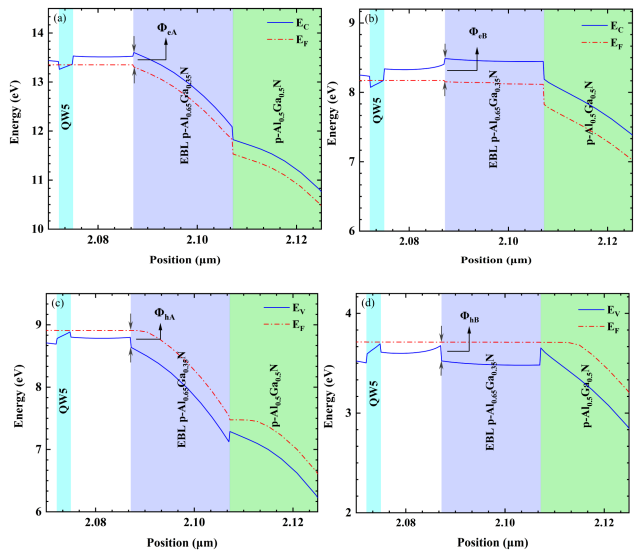

Fig. 4. Conduction band diagrams of (a) Sample A and (b) Sample B at 120 mA. Valence band diagrams of (c) Sample A and (d) Sample B at 120 mA.

(b), the electrons and holes concentration in the active region of Sample B are both higher than those of Sample A, which is benefited from the improvement of electron blocking and hole injection ability. Fig. 3(c) shows the normalized electron currents of the two samples. Compared with Sample A,the leakage current in the p-type region of Sample B decreases from 50% to 2%. Since IP is in the EBL, we believe that the improved performance originates from the change of the energy band of the EBL. To explain the potential boosting mechanism, the band diagrams of Sample A and B at 120 mA are plotted in Fig. 4. Solid blue lines are energy bands, and red dot dashed lines are quasi-Fermi levels. To quantitatively analyze the ability of electron blocking and hole injection, Φ_e is used to represent the energy difference between quasi-Fermi level and conduction band, while Φ_h represents the energy difference between quasi-Fermi level and valence band. The Φ_{eA} and Φ_{hA} for Sample A are 293.1 meV and 271.0 meV, respectively, while the Φ_{eB} and Φ_{hB} for Sample B are 335.4 meV and 188.7 meV, respectively. Compared with Sample A, the electron barrier in Sample B is increased by 42.3 meV, thus the electron leakage is suppressed more. At the same time, the hole barrier in Sample B is reduced by 82.3 meV compared with Sample A, so the hole injection becomes easier. Ultimately, the increased electron and hole concentrations in MQWs of Sample B can be explained.

To further verify the origin of improved performance of the device, the distance between IP and SP is increased to be 20 nm. At that point IP is no longer in the EBL, but at the interface between EBL and p-$Al_{0.5}Ga_{0.5}N$, and this structure is denoted as Sample C. Fig. 5 shows the calculation results of Sample C. At 120 mA, the voltage and LOP of Sample C is 9.58V and 29.77mW, respectively. Compared with Sample A, the improvement of Sample C is lower than that of Sample B. Similarly, we plot the energy band diagram of Sample C, and the Φ_{eC} and Φ_{hC} are 309.9 meV and 245.2 meV, respectively. Compared with Sample A, the Φ_e increases by 16.8 meV, and the Φ_h decreases by 25.8 meV. The Φ_{eC} is lower than Φ_{eB}, while the Φ_{hC} is higher than Φ_{hB}, thus the performance improvement of Sample C is inferior than that of Sample B. This can further prove that LOP is improved as a result of the increased electron barrier and the decreased hole barrier.

To further investigate how the polarity inversion induces reduction of the bias voltage, the valence bands of the three samples without bias voltage are plotted, as shown in Fig. 6. It is believed that the hole barriers in the p-type region influence the bias voltage of device. The height of hole barrier between the EBL and p-$Al_{0.5}Ga_{0.5}N$ is defined as $\Delta h1$, and that between the p-$Al_{0.5}Ga_{0.5}N$ and p-GaN is defined as $\Delta h2$. The values of $\Delta h1$ and $\Delta h2$ of the three samples are shown in

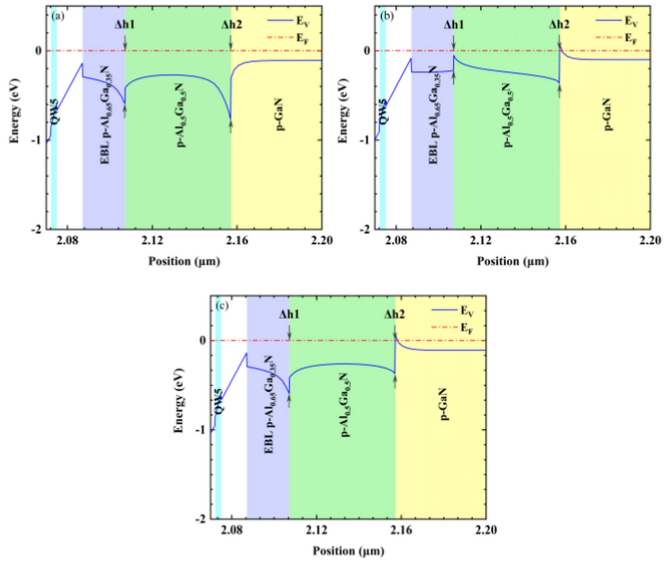

Fig. 6. (a) Valence band diagrams of (a) Sample A, (b) Sample B and (c) Sample C without bias voltage.

TABLE I
SIMULATED POTENTIAL BARRIER OF HOLES FOR THREE SAMPLES

Sample	Holes BarrierΔh1	Holes BarrierΔh2
Sample A	590.8 meV	765.8 meV
Sample B	223.3 meV	362.0 meV
Sample C	590.6 meV	368.8 meV

Table I. The Δh1 of Sample A and C are the same and higher than the Δh1 of Sample B. The Δh2 of Sample B and C are similar and lower than the Δh2 of Sample A. Compared with Sample A, Sample B and C have different variations on Δh1 and the same variation on Δh2, which indicates Δh1 has no effect on the bias voltage, and that the reduction of the bias voltage is mainly due to the reduced Δh2. The reduced Δh2 is because of the different polarization charges at the interface between p-$Al_{0.5}Ga_{0.5}N$ and p-GaN. For Sample A, the polarization charges at the interface between p-$Al_{0.5}Ga_{0.5}N$ and p-GaN are positive, which can deplete the holes, accounting for the high hole barrier. The hole injection regions of Sample B and C are Ga-polar, the charges at the interface between p-$Al_{0.5}Ga_{0.5}N$ and p-GaN become negative charges, which enhances hole accumulation and effectively reduces the hole barrier compared with Sample A [14].

Furthermore, the two structures are simulated where the distance between IP and SP are 30 nm and 50 nm, respectively. The same energy band and output performance as Sample C are obtained. However, when the distance between IP and SP exceeds 70 nm, the performance of the device will not be improved. Therefore, IP should be in the EBL or p-$Al_{0.5}Ga_{0.5}N$.

The structures discussed above have the hole injection layer with the same doping concentration and the ionization rate. However, in actual production, the hole concentration in N-polar GaN will be reduced due to the effect of oxygen impurity [31]. If the range of background electron concentration generated by oxygen impurity is about 1×10^{17} cm^{-3} [21], [32], the hole concentration of p-GaN in Sample A should be reduced to 1.5×10^{17} cm^{-3}. This structure is denoted as Sample D. At the same time, the hole concentration of p-GaN in the samples with polarity inversion remains unchanged. Considering the quality of epitaxial layers in actual production, the structure with 50nm distance between IP and SP is selected, and this structure is denoted as Sample E. The simulation results of Sample D and E are shown in Fig. 7. Relative to Sample D, the LOP of Sample E increases from 21.34 mW to 29.71 mW, and the applied voltage reduces from 16.06 V to 9.63 V at 120 mA. As a result, the WPE of Sample E is boosted by about 132% at 120 mA. It can be concluded that the efficiency of the DUV LEDs with polarity inversion will achieve more improvements in practical applications.

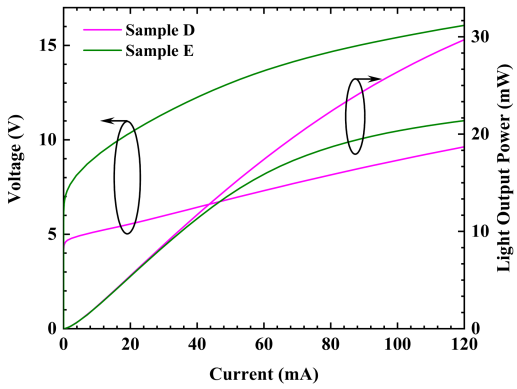

Fig. 7. I-V and L-I curves of Sample D and E.

IV. CONCLUSION

In summary, we have investigated the effect of polarity inversion of the hole injection layer on N-polar 274-nm DUV LED. The electron barrier increases and the hole barrier decreases due to the polarity inversion. Therefore, the structure with polarity inversion increases hole injection and decreases electron leakage compared with the original structure without polarity inversion. In addition, under the same injection current, the large reduction in bias voltage results in a significant enhancement of WPE. Finally, we design an optimized structure which has a suitable inversion position. At 120 mA, the LOP of the optimized structure is boosted by 39.2% and the WPE is boosted by 132% compared with the original structure whose growth direction is completely along [000-1] direction. Therefore, it is believed polarity inversion is an effective way to realize DUV LEDs with excellent performance.

REFERENCES

[1] S. Rattanakul and K. Oguma, "Analysis of hydroxyl radicals and inactivation mechanisms of bacteriophage MS2 in response to a simultaneous application of UV and chlorine," *Environ. Sci. Technol.*, vol. 51, no. 1, pp. 455–462, Jan. 2017, doi: 10.1021/acs.est.6b03394.

[2] S. Rattanakul and K. Oguma, "Inactivation kinetics and efficiencies of UV-LEDs against Pseudomonas aeruginosa, Legionella pneumophila, and surrogate microorganisms," *Water Res.*, vol. 130, pp. 31–37, Mar. 2018, doi: 10.1016/j.watres.2017.11.047.

[3] H. Okamura, S. Niizeki, T. Ochi, and A. Matsumoto, "UV curable formulations for UV-C LEDs," *J. Photopolymer Sci. Technol.*, vol. 29, no. 1, pp. 99–104, 2016, doi: 10.2494/photopolymer.29.99.

[4] M. Nakamura, A. Morita, S. Seite, T. Haarmann-Stemmann, S. Grether-Beck, and J. Krutmann, "Environment-induced lentigines: Formation of solar lentigines beyond ultraviolet radiation," *Exp. Dermatol.*, vol. 24, no. 6, pp. 407–411, Jun. 2015, doi: 10.1111/exd.12690.

[5] H. Hirayama, N. Maeda, S. Fujikawa, S. Toyoda, and N. Kamata, "Recent progress and future prospects of ALGaN-based high-efficiency deep-ultraviolet light-emitting diodes," *Japanese J. Appl. Phys.*, vol. 53, no. 10, Oct. 2014, Art. no. 100209, doi: 10.7567/jjap.53.100209.

[6] T. Takano, T. Mino, J. Sakai, N. Noguchi, K. Tsubaki, and H. Hirayama, "Deep-ultraviolet light-emitting diodes with external quantum efficiency higher than 20% at 275 nm achieved by improving light-extraction efficiency," *Appl. Phys. Exp.*, vol. 10, no. 3, Mar. 2017, Art. no. 031002, doi: 10.7567/apex.10.031002.

[7] H. Hirayama et al., "222-282 nm AlGaN and InAlGaN-based deep-UV LEDs fabricated on high-quality AlN on sapphire," *Physica Status Solidi a-Appl. Mater. Sci.*, vol. 206, no. 6, pp. 1176–1182, Jun. 2009, doi: 10.1002/pssa.200880961.

[8] J. Simon, V. Protasenko, C. X. Lian, H. L. Xing, and D. Jena, "Polarization-Induced hole doping in wide-band-gap uniaxial semiconductor heterostructures," *Science*, vol. 327, no. 5961, pp. 60–64, Jan. 2010, doi: 10.1126/science.1183226.

[9] H. Hirayama, Y. Tsukada, T. Maeda, and N. Kamata, "Marked enhancement in the efficiency of deep-ultraviolet AlGaN light-emitting diodes by using a multiquantum-barrier electron blocking layer," *Appl. Phys. Exp.*, vol. 3, no. 3, 2010, Art. no. 031002, doi: 10.1143/apex.3.031002.

[10] H. Y. Ryu, I. G. Choi, H. S. Choi, and J. I. Shim, "Investigation of light extraction efficiency in AlGaN deep-ultraviolet light-emitting diodes," *Appl. Phys. Exp.*, vol. 6, no. 6, Jun. 2013, Art. no. 062101, doi: 10.7567/apex.6.062101.

[11] H. K. Su et al., "Improving the current spreading by Fe doping in n-GaN layer for GaN-Based ultraviolet light-emitting diodes," *IEEE Electron Device Lett.*, vol. 42, no. 9, pp. 1346–1349, Sep. 2021, doi: 10.1109/led.2021.3100545.

[12] F. B. Liao et al., "The effects of polarization-modulated quaternary AlInGaN barriers in Deep-UV-LED," *J. Electron. Mater.*, vol. 51, no. 1, pp. 126–132, Jan, 2022, doi: 10.1007/s11664-021-09272-1.

[13] F. Akyol, D. N. Nath, S. Krishnamoorthy, P. S. Park, and S. Rajan, "Suppression of electron overflow and efficiency droop in N-polar GaN green light emitting diodes," *Appl. Phys. Lett.*, vol. 100, no. 11, Mar. 2012, Art. no. 111118, doi: 10.1063/1.3694967.

[14] H. C. Tao, S. R. Xu, X. M. Fan, J. C. Zhang, and Y. Hao, "Greatly enhanced wall-plug efficiency of N-polar AlGaN-Based deep ultraviolet light-emitting diodes," *IEEE Photon. J.*, vol. 13, no. 3, Jun. 2021, Art. no. 8200311, doi: 10.1109/jphot.2021.3084752.

[15] Z. Zhuang, D. Iida, and K. Ohkawa, "Enhanced performance of N-polar AlGaN-Based deep-ultraviolet light-emitting diodes," *Opt. Exp.*, vol. 28, no. 21, pp. 30423–30431, Oct. 2020, doi: 10.1364/oe.403168.

[16] Y. B. Zhao et al., "Performance enhancement of an N-polar nitride deep-ultraviolet light-emitting diode with compositionally graded p-AlGaN," *Opt. Lett.*, vol. 47, no. 2, pp. 385–388, Jan, 2022, doi: 10.1364/ol.449099.

[17] Y. F. Li, Y. Jiang, H. Q. Jia, W. X. Wang, R. Yang, and H. Chen, "Superior optoelectronic performance of N-Polar GaN LED to Ga-polar counterpart in the 'Green gap' range," *IEEE Access,* vol. 10, pp. 95565–95570, 2022, doi: 10.1109/access.2022.3204668.

[18] S. Keller et al., "Influence of the substrate misorientation on the properties of N-polar InGaN/GaN and AlGaN/GaN heterostructures," *J. Appl. Phys.*, vol. 104, no. 9, Nov. 2008, Art. no. 093510, doi: 10.1063/1.3006132.

[19] D. Won, X. J. Weng, and J. M. Redwing, "Metalorganic chemical vapor deposition of N-polar GaN films on vicinal SiC substrates using indium surfactants," *Appl. Phys. Lett.*, vol. 100, no. 2, Jan. 2012, Art. no. 021913, doi: 10.1063/1.3676275.

[20] X. W. Wang et al., "Optimization of N-polar GaN growth on bulk GaN substrate by MOCVD," *Mater. Lett.*, vol. 253, pp. 314–316, Oct. 2019, doi: 10.1016/j.matlet.2019.06.106.

[21] N. A. Fichtenbaum, T. E. Mates, S. Keller, S. P. DenBaars, and U. K. Mishra, "Impurity incorporation in heteroepitaxial N-face and Ga-face GaN films grown by metalorganic chemical vapor deposition," *J. Cryst. Growth*, vol. 310, no. 6, pp. 1124–1131, Mar. 2008, doi: 10.1016/j.jcrysgro.2007.12.051.

[22] A. J. Ptak et al., "Controlled oxygen doping of GaN using plasma assisted molecular-beam epitaxy," *Appl. Phys. Lett.*, vol. 79, no. 17, pp. 2740–2742, Oct. 2001, doi: 10.1063/1.1403276.

[23] M. H. Wong, F. Wu, T. E. Mates, J. S. Speck, and U. K. Mishra, "Polarity inversion of N-face GaN by plasma-assisted molecular beam epitaxy," *J. Appl. Phys.*, vol. 104, no. 9, Nov. 2008, Art. no. 093710, doi: 10.1063/1.3009669.

[24] S. Pezzagna, P. Vennegues, N. Grandjean, and J. Massies, "Polarity inversion of GaN(0001) by a high Mg doping," *J. Cryst. Growth*, vol. 269, no. 2-4, pp. 249–256, Sep. 2004, doi: 10.1016/j.jcrysgro.2004.05.067.

[25] N. Grandjean, A. Dussaigne, S. Pezzagna, and P. Vennegues, "Control of the polarity of GaN films using an Mg adsorption layer," *J. Cryst. Growth*, vol. 251, no. 1/4, pp. 460–464, Apr. 2003, doi: 10.1016/s0022-0248(02)02361-8.

[26] V. Ramachandran et al., "Inversion of wurtzite GaN(0001) by exposure to magnesium," *Appl. Phys. Lett.*, vol. 75, no. 6, pp. 808–810, Aug. 1999, doi: 10.1063/1.124520.

[27] J. E. Northrup, "Magnesium incorporation at (0001) inversion domain boundaries in GaN," *Appl. Phys. Lett.*, vol. 82, no. 14, pp. 2278–2280, Apr. 2003, doi: 10.1063/1.1565707.

[28] I. Vurgaftman, J. R. Meyer, and L. R. Ram-Mohan, "Band parameters for III-V compound semiconductors and their alloys," *J. Appl. Phys.*, vol. 89, no. 11, pp. 5815–5875, Jun. 2001, doi: 10.1063/1.1368156.

[29] J. Piprek, "Efficiency droop in nitride-based light-emitting diodes," *Physica Status Solidi a-Appl. Mater. Sci.*, vol. 207, no. 10, pp. 2217–2225, Oct. 2010, doi: 10.1002/pssa.201026149.

[30] V. Fiorentini, F. Bernardini, and O. Ambacher, "Evidence for nonlinear macroscopic polarization in III-V nitride alloy heterostructures," *Appl. Phys. Lett.*, vol. 80, no. 7, pp. 1204–1206, Feb. 2002, doi: 10.1063/1.1448668.

[31] S. Keller et al., "Recent progress in metal-organic chemical vapor deposition of N-polar group-III nitrides," *Semicond. Sci. Technol.*, vol. 29, no. 11, Nov. 2014, Art. no. 113001, doi: 10.1088/0268-1242/29/11/113001.

[32] L. K. Li, M. J. Jurkovic, W. I. Wang, J. M. Van Hove, and P. P. Chow, "Surface polarity dependence of Mg doping in GaN grown by molecular-beam epitaxy," *Appl. Phys. Lett.*, vol. 76, no. 13, pp. 1740–1742, Mar. 2000, doi: 10.1063/1.126152.